VIP Vibrational Spectroscopy

DOI: 10.1002/ange.201102846

Distribution Pattern of Length, Length Uniformity, and Density of TiO_3^{2-} Quantum Wires in an ETS-10 Crystal Revealed by Laser-Scanning Confocal Polarized Micro-Raman Spectroscopy**

*Nak Cheon Jeong, Hyunjin Lim, Hyeonsik Cheong, and Kyung Byung Yoon**

ETS-10 is a highly intriguing microporous titanosilicate[1–3] that has shown an excellent propensity for the selective removal of harmful heavy-metal ions,[4–9] the potential to work as an effective catalyst for various reactions,[10–15] and that can be used as a material for solar cells.[16] Such important features arise from the TiO_3^{2-} quantum wires with the diameter (d) of approximately 0.67 nm running along the [110] and [1$\bar{1}$0] directions in the crystal (Figure 1).[1–3,17–27] The TiO_3^{2-} quantum wire is a one-dimensional (1D) extreme of three-dimensional (3D) bulk titanates, which are widely used in industry as, for example, capacitors.[28] It also exhibits an interesting 1D quantum confinement effect.[17]

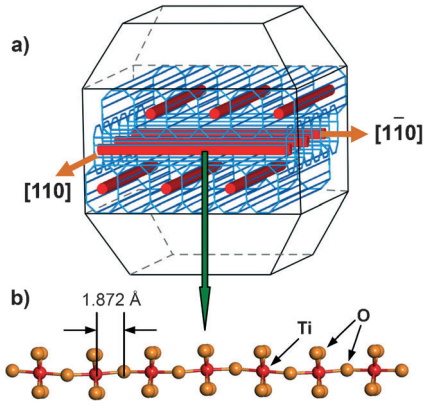

Figure 1. a) Illustrations of a typical morphology (truncated bipyramid) of an ETS-10 crystal and three-dimensional networks of SiO_2 channels (cyan) and TiO_3^{2-} quantum wires (red) in the case of polymorph B and b) a single TiO_3^{2-} quantum wire.

The TiO_3^{2-} quantum wires are not expected to be connected all the way from one face to the opposite face of a crystal owing to the large number of randomly distributed defects.[17–22,29–37] Now the questions are what is the average length of the wires, to what degree do the lengths vary (how does the length homogeneity vary), how does the local density of the quantum wire vary from one region to another within a crystal, do they vary randomly or in accordance with a certain pattern? Answers to the above questions will be highly useful for understanding the mechanism of ETS-10 formation and growth, the refinement of its structure, improvements of its catalytic activities, and its future applications. However, there have been no methods to gain such information.

The TiO_3^{2-} quantum wire in ETS-10 gives a strong Raman shift band between 724 and 840 cm^{-1}, arising from a longitudinal vibrational mode of the -Ti-O-Ti-O- chain. Its frequency at the band maximum (ν_{max}), its bandwidth (full width at half maximum, fwhm), and intensity (I) reflect the relative average length, length homogeneity, and density of the quantum wire, respectively. The Raman band frequency decreases as the length increases, owing to the increase in the reduced mass of the quantum wire. The smallest frequency ever observed is 724 cm^{-1}.

Bandwidths between 23 and 120 cm^{-1} have been observed, and the bandwidth decreases as the length uniformity increases. The intensity increases as the number of the TiO_3^{2-} quantum wire increases. Accordingly, the frequency, bandwidth, and intensity have served as the three important criteria for comparison of the relative average lengths, relative average length uniformities, and relative average densities of the TiO_3^{2-} quantum wires in the ETS-10 crystals. This information indicates that we can also apply the same principle to obtain their distribution pattern within an ETS-10 crystal if we can obtain a matrix of Raman spectra measured from a large number of artificially divided very small sections of a crystal. Furthermore, the obtained data would be more informative if we can obtain a map of these three data sets for the TiO_3^{2-} quantum wires running along the [110] and [1$\bar{1}$0] directions, respectively.

We now report that laser scanning confocal polarized micro-Raman (LSC-PMR) spectroscopy is a highly useful tool for the above purpose and the novel fact that the TiO_3^{2-} quantum wires are not evenly distributed within ETS-10 crystals but distributed in a symmetrical manner according to an interesting pattern.

[*] Dr. N. C. Jeong,[++] Prof. Dr. K. B. Yoon
Korea Center for Artificial Photosynthesis and
Department of Chemistry, Sogang University
Seoul 121-742 (Korea)
E-mail: yoonkb@sogang.ac.kr
Dr. H. Lim,[+] [++] Prof. Dr. H. Cheong
Department of Physics, Sogang University
Seoul 121-742 (Korea)
[+] Current address: Agency for Defense Development
Daejeon 305-152 (Korea)
[++] These authors contributed equally to this work.

[**] We thank the Korea Center for Artificial Photosynthesis located in Sogang University and funded by MEST through the National Research Foundation of Korea (NRF-2009-C1 AA A001-2009-0093879). We also thank Jiyoon Lee for providing us the graphics. H.C. further thanks the Future-Based Technology Development Program (Nano Fields) of the NRF funded by the MEST (2008-2004744).

Supporting information for this article is available on the WWW under http://dx.doi.org/10.1002/anie.201102846.

ETS-10 crystals with a size of 20 μm were prepared according to the reported procedure.[17] The scanning electron microscopy (SEM) and optical microscopy images of a typical crystal (Figure 2a,b) show that the ETS-10 crystals used in this work are highly crystalline and that their surfaces are smooth. All the LSC-PMR data were obtained from ETS-10 crystals with their *c* axes pointing up (details of the procedure in the Supporting Information, SI-1). The LSC-PMR data were collected from a home-built system equipped with a nanostage, a spectrometer, a CCD detector, and an Ar^+ ion laser (details of the configuration in the Supporting Information, SI-2). The wavelength of the excitation beam was 514.5 nm and the beam was focused with the diameter of 700 nm. The nanostage was moved vertically and horizontally by 500 nm. The spatial precision of the nanostage was approximately 100 nm.

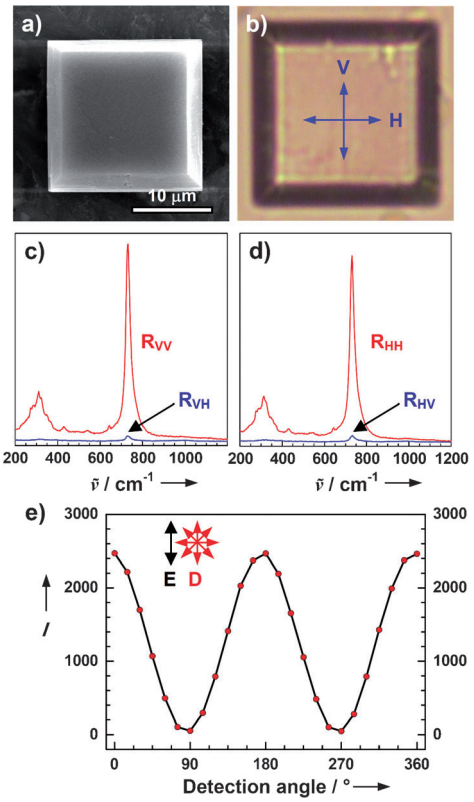

Figure 2. a) Scanning electron microscopy and b) optical microscopy images of an ETS-10 crystal mounted on a glass cover plate. c,d) Raman spectra of the center of the crystal for the cases of VV and VH (c) and HH and HV (d). e) Variation of the intensity of the longitudinal vibration of the TiO_3^{2-} quantum wire with respect to the angle θ between the polarization direction of the excitation beam (E) and the direction of the polarizer placed in front of the detector (D).

A data set of 1600 (40 × 40) spatially resolved Raman spectra was obtained from a 20 μm ETS-10 crystal for the four different cases of combination between the sheet polarization of the excitation beam and the orientation of the sheet polarizer in front of the detector, namely, vertical/vertical (VV), vertical/horizontal (VH), horizontal/horizontal (HH), and horizontal/vertical (HV). Thus, 6400 spatially resolved micro-Raman spectra were collected from each crystal. The frequency (ν_{max}), bandwidth (fwhm), and intensity of the longitudinal vibration band were extracted from each data set. Thus, a total of 19200 data points was obtained from an ETS-10 crystal.

As a test case, four Raman spectra were obtained from the center of a 20 μm crystal for the four different cases of VV, VH, HH, and HV (Figure 2c,d). The corresponding Raman spectra are denoted as R_{VV}, R_{VH}, R_{HH}, R_{HV}, respectively. The intensities of the longitudinal vibrations of the TiO_3^{2-} quantum wires were 2460 (R_{VV}), 28 (R_{VH}), 2320 (R_{HH}), and 26 (R_{HV}) cps (counts per second). The intensity ratios were 87 and 89 for VV/VH and HH/HV, respectively, thus indicating that the LSC-PMR spectrometer works well and records the Raman spectra only from the TiO_3^{2-} quantum wires running along the [110] and [1$\bar{1}$0] directions. Conversely, this result confirms that the TiO_3^{2-} quantum wires indeed run along the [110] and [1$\bar{1}$0] directions. For a fixed vertical laser excitation, the variation of the vibrational intensity of TiO_3^{2-} quantum wires in response to the change of the orientation angle of the polarizer placed in front of the detector is shown in Figure 2e. This result further shows that the intensity of the longitudinal vibration of the TiO_3^{2-} quantum wire varies according to $\cos^2\theta$, where θ is the angle between the polarization direction of the excitation beam and the direction of the polarizer placed in front of the detector.

The two-dimensional (2D) frequency (ν_{max}) maps of the longitudinal vibration are shown in Figure 3a,b, for the two cases of VV and HH. The result shows that the frequency varies slightly between 727 and 731 cm^{-1} over the entire crystal. This result indicates that the length variation is not significant in the case of the ETS-10 crystal used in this study and that the lengths of the TiO_3^{2-} quantum wires are

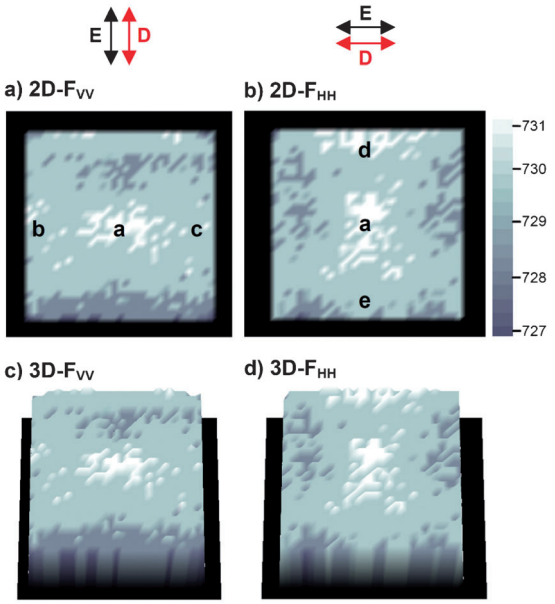

Figure 3. 2D frequency (ν_{max}) maps of the longitudinal vibration of the TiO_3^{2-} quantum wire at its maximum for the cases of a) VV and b) HH and the corresponding 3D maps for the cases of c) VV and d) HH.

somewhat shorter than the longest one ever observed before, whose vibrational frequency was 724 cm^{-1}. Although the frequency difference is not large, we could detect that the frequencies of the TiO_3^{2-} quantum wires located at the center (region a) and those that are vertically aligned at the left (region b) and right (region c) edges in the case of VV (Figure 3a) and those that are horizontally aligned at the top (region d) and bottom (region e) edges in the case of HH (Figure 3b) are higher than the rest of the regions. This finding indicates that, although the difference is small, the lengths of the TiO_3^{2-} quantum wires located at the center, the vertically running quantum wires located at b and c regions, and the horizontally running quantum wires located at d and e regions are shorter than quantum wires located in other regions. The 3D frequency maps of the longitudinal vibration viewed from the *c* axis shown in Figure 3c,d show the above phenomenon more clearly.

The 2D and 3D bandwidth (fwhm) maps of the longitudinal vibration are shown in Figure 4a–d for the two cases of VV and HH, respectively. The 2D maps (Figure 4a,b) very much resemble hourglasses, as the upper and lower isosceles triangles are darker than the left and right isosceles triangles in the case of VV (Figure 4a); the opposite is the case for HH polarization (Figure 4b). The 3D bandwidth maps of the longitudinal vibration (Figure 4c,d) show more details of its bandwidth profiles. The numbers shown on the 3D intensity maps represent the bandwidths (in cm^{-1}) at the corresponding spots. Thus, the bandwidth decreases in the order spot e > spot d > spot c > spot b > spot a, where the labels represent the spots shown in the 2D maps (Figure 4a,b). This result shows that an ETS-10 crystal can be divided into four domains, each of which has the shape of an isosceles triangular prism (Figure 4e,f) based on the distribution pattern of length homogeneity of the TiO_3^{2-} quantum wires. Figure 4e shows the TiO_3^{2-} quantum wires running perpendicular to the side face [(110) or (1$\bar{1}$0) plane] and Figure 4f shows the TiO_3^{2-} quantum wires running parallel to the side face in each isosceles triangular prismatic piece. They are denoted as "perpendicular" and "parallel" TiO_3^{2-} quantum wires, respectively. The results show the important fact that the length homogeneity of the perpendicular wires is higher than that of the parallel wires in each isosceles triangular prismatic piece. It also shows that the length homogeneity is highest at the 45° corner (spot a or c) and lowest at the 90° corner (near spot e) in each case (Figure 4c,d). It is also interesting to note that the bandwidths at spots a and b (22.2 and 22.8 cm^{-1}) are smaller than the smallest value ever observed (24 cm^{-1}).

The 2D intensity (*I*) maps of the longitudinal vibration are shown in Figure 5a,b for the two cases of VV and HH. The 2D intensity maps also show hourglass images, which are more distinctive than the 2D bandwidth maps (Figure 4a,b), owing to the larger differences in bandwidth values. The 3D intensity maps of the longitudinal vibration shown in Figure 5c,d show more details of its intensity profiles viewed from the *c* axis. The numbers on the 3D intensity maps represent the intensities (in cps) at the corresponding spots. In contrast, the corresponding images for the cases of VH and HV do not reveal much information owing to the very weak intensities for these polarizations (SI-3 in the Supporting Information).

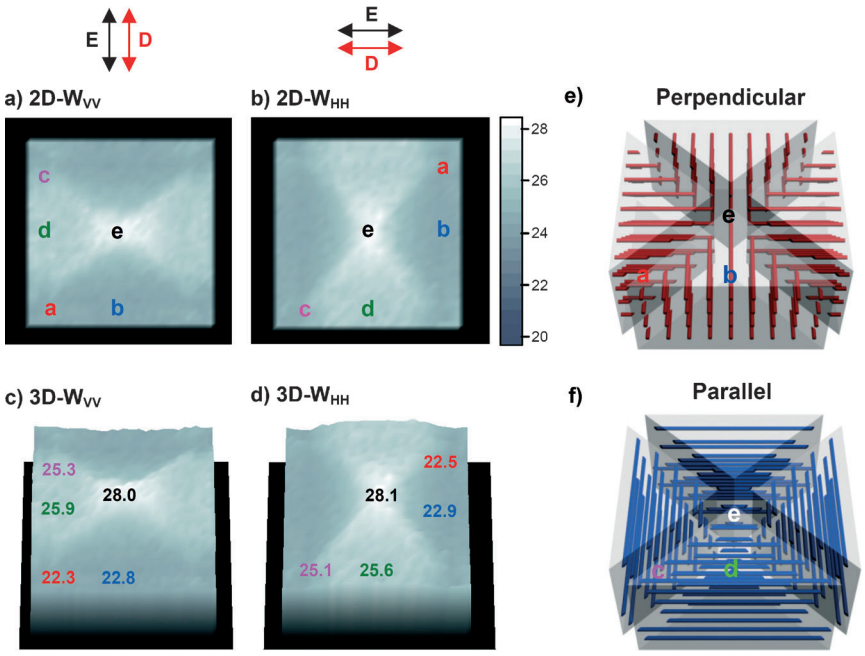

Figure 4. 2D bandwidth (fwhm) maps of the longitudinal vibration of the TiO_3^{2-} quantum wire for the cases of a) VV and b) HH and the corresponding 3D maps for the cases of c) VV and d) HH and the illustration of the e) perpendicular and f) parallel TiO_3^{2-} quantum wires.

The above three sets of data reveal interesting facts. The length, length homogeneity, and density of TiO_3^{2-} quantum wires are not evenly distributed within an ETS-10 crystal. When viewed along the *c* axis, an ETS-10 crystal can be divided into four equivalent isosceles triangular prismatic domains by dividing the crystal with two diagonal lines based on the length homogeneity and density of the TiO_3^{2-} quantum wires. The 2D frequency maps can also be divided by the two diagonal lines as shown in SI-4 in the Supporting Information. Accordingly, the lengths of the perpendicular wires are slightly longer than those of the parallel wires. More distinctively, the length homogeneity and density of the perpendicular wires are higher than those of the parallel wires in each isosceles triangular prismatic domain. The density of the TiO_3^{2-} quantum wires, their length homogeneity, and length gradually increase on going from the 90° corner (spot e, the center of the crystal) to the side face in each isosceles triangular domain. This phenomenon is more pronounced in the case of the perpendicular wires. The density of the quantum wires and length homogeneity gradually decrease on going from the

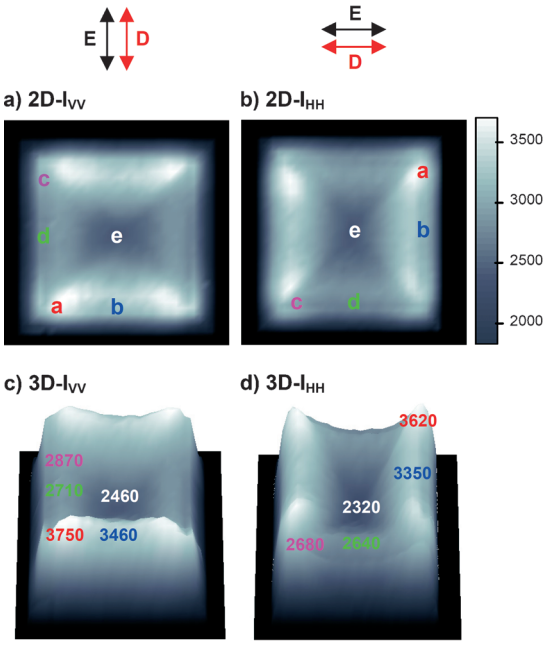

Figure 5. 2D intensity maps of the longitudinal vibration of the TiO_3^{2-} quantum wire for the cases of a) VV and b) HH and the corresponding 3D maps for the cases of c) VV and d) HH.

45° corner to the middle (spot a→spot b and spot c→spot d). Thus, at the center, the lengths of the TiO_3^{2-} quantum wires are shortest, the length homogeneity is lowest, and the density of the TiO_3^{2-} quantum wires is lowest. Likewise, we propose that the silica channel density and the degree of the channel length homogeneity increase on going from the center (90° corner) to the edge and from the middle to the 45° corner along the long edge.

The above information will be highly useful for the study of the mechanism of the ETS-10 crystal growth and the application of ETS-10 for various purposes. Furthermore, since the density of the TiO_3^{2-} quantum wire and the length homogeneity of the quantum wires reflect the crystallinity, the above data further allow us to reveal the important phenomenon that in ETS-10 the crystallinity increases on going from the center to the edge and on going from the middle to the corner along the edge. In particular, the crystallinity in the direction of the crystal growth increases. We attribute the above phenomenon to the presence of two steps in the crystallization process, namely, the initial autogeneses seed formation step (primary growth) and the secondary crystal growth step (secondary growth), and to the decrease of the crystal growth rate as the size of the crystal increases caused by the decrease of the concentration of nutrients as the crystal size increases. Thus the autogenously formed seed crystals are likely to have relatively larger degrees of defects because the seed crystals have to be formed in the absence of any crystal pattern. The part of the crystal that is added onto the autogenously formed seed crystal is likely to have lower amounts of defects, because the growth takes place onto the existing crystal pattern. The amounts of defect are likely to decrease as the growth rate decreases, which will decrease as the concentrations of the nutrients in the gel decrease, as is the usual case for the synthesis of zeolites by batch reactions.

This work gives insights into the distributions of the relative length, relative length homogeneity, and relative density of the TiO_3^{2-} quantum wires in ETS-10 crystals (SI-5 in the Supporting Information), and into the distribution mode of defects in zeolites. These findings will help ETS-10 be better understood and facilitate its use for various applications. This work also demonstrates the usefulness of the application of LSC-PMR spectroscopy for the elucidation of the unprecedented important properties of zeolites if they are Raman-active species or have Raman-active adsorbed or encapsulated guest species. Together with laser scanning confocal fluorescence microscopy (LSC-FM),[38] the use of LSC-PMR will be an important addition to the zeolite research.

Received: April 25, 2011
Published online: July 22, 2011

Keywords: ETS-10 · Raman spectroscopy · silicates · spatially resolved spectroscopy · structure elucidation

[1] S. M. Kuznicki, US Patent 4853202, **1989**.
[2] M. W. Anderson, O. Terasaki, T. Ohsuna, A. Philippou, S. P. MacKay, A. Ferreira, J. Rocha, S. Lidin, *Nature* **1994**, *367*, 347–351.
[3] M. W. Anderson, O. Terasaki, T. Ohsuna, P. J. O. Malley, A. Philippou, S. P. MacKay, A. Ferreira, J. Rocha, S. Lidin, *Philos. Mag. B* **1995**, *71*, 813–841.
[4] L. Lv, G. Tsoi, X. S. Zhao, *Ind. Eng. Chem. Res.* **2004**, *43*, 7900–7906.
[5] X. S. Zhao, J. L. Lee, P. A. Chia, *Langmuir* **2003**, *19*, 1977–1979.
[6] L. Lv, K. Wang, X. S. Zhao, *J. Colloid Interface Sci.* **2007**, *305*, 218–225.
[7] J. H. Choi, S. D. Kim, S. H. Noh, S. J. Oh, W. J. Kim, *Microporous Mesoporous Mater.* **2006**, *87*, 163–169.
[8] J. H. Choi, S. D. Kim, Y. J. Kwon, W. J. Kim, *Microporous Mesoporous Mater.* **2006**, *96*, 157–167.
[9] C. B. Lopes, M. Otero, J. Coimbra, E. Pereira, J. Rocha, Z. Lin, A. Duarte, *Microporous Mesoporous Mater.* **2007**, *103*, 325–332.
[10] A. Philippou, M. Naderi, J. Rocha, M. W. Anderson, *Catal. Lett.* **1998**, *53*, 221–224.
[11] A. Philippou, M. W. Anderson, *J. Catal.* **2000**, *189*, 395–400.
[12] A. Valente, Z. Lin, P. Brandão, I. Portugal, M. W. Anderson, J. Rocha, *J. Catal.* **2001**, *200*, 99–105.
[13] E. J. Doskocil, *J. Phys. Chem. B* **2005**, *109*, 2315–2320.
[14] S. B. Waghmode, R. Vetrivel, C. S. Gohinath, S. Sivasanker, *J. Phys. Chem. B* **2004**, *108*, 11541–11548.
[15] V. Luca, M. Osborne, D. Sizgek, C. Griffith, P. Z. Araujo, *Chem. Mater.* **2006**, *18*, 6132–6138.
[16] P. Atienzar, S. Valencia, A. Corma, H. Garcia, *ChemPhysChem* **2007**, *8*, 1115–1119.
[17] N. C. Jeong, M. H. Lee, K. B. Yoon, *Angew. Chem.* **2007**, *119*, 5972–5976; *Angew. Chem. Int. Ed.* **2007**, *46*, 5868–5872.
[18] N. C. Jeong, Y. J. Lee, J.-H. Park, H. Lim, C.-H. Shin, H. Cheong, K. B. Yoon, *J. Am. Chem. Soc.* **2009**, *131*, 13080–13092.
[19] N. C. Jeong, Y. J. Lee, K. B. Yoon, *Microporous Mesoporous Mater.* **2008**, *115*, 308–313.
[20] F. X. Llabrés i Xamena, A. Damin, S. Bordiga, A. Zecchina, *Chem. Commun.* **2003**, 1514–1515.

[21] A. Damin, F. X. Llabrés i Xamena, C. Lamberti, B. Civalleri, C. M. Zicovich-Wilson, A. Zecchina, *J. Phys. Chem. B* **2004**, *108*, 1328 – 1336.
[22] B. Yilmaz, J. Warzywoda, A. Sacco Jr. , *Nanotechnology* **2006**, *17*, 4092 – 4099.
[23] E. Borello, C. Lamberti, S. Bordiga, A. Zecchina, C. O. Areán, *Appl. Phys. Lett.* **1997**, *71*, 2319 – 2321.
[24] S. Bordiga, G. T. Palomino, A. Zecchina, G. Ranghino, E. Giamello, C. Lamberti, *J. Chem. Phys.* **2000**, *112*, 3859 – 3867.
[25] A. M. Zimmerman, D. J. Doren, R. F. Lobo, *J. Phys. Chem. B* **2006**, *110*, 8959 – 8964.
[26] C. Lamberti, *Microporous Mesoporous Mater.* **1999**, *30*, 155 – 163.
[27] X. Wang, A. J. Jacobson, *Chem. Commun.* **1999**, 973 – 974.
[28] D. V. Bavykin, J. M. Friedrich, F. C. Walsh, *Adv. Mater.* **2006**, *18*, 2807 – 2824.
[29] Y. K. Krisnandi, E. E. Lachowski, R. F. Howe, *Chem. Mater.* **2006**, *18*, 928 – 933.
[30] P. D. Southon, R. F. Howe, *Chem. Mater.* **2002**, *14*, 4209 – 4218.
[31] C. C. Pavel, B. Zibrowius, E. Löffler, W. Schmidt, *Phys. Chem. Chem. Phys.* **2007**, *9*, 3440 – 3446.
[32] B. Mihailova, V. Valtchev, S. Mintova, L. Konstantinov, *Zeolites* **1996**, *16*, 22 – 24.
[33] C. C. Pavel, S.-H. Park, A. Dreier, B. Tesche, W. Schmidt, *Chem. Mater.* **2006**, *18*, 3813 – 3820.
[34] L. Lv, J. K. Zhou, F. Su, X. S. Zhao, *J. Phys. Chem. C* **2007**, *111*, 773 – 778.
[35] Y. Su, M. L. Balmer, B. C. Bunker, *J. Phys. Chem. B* **2000**, *104*, 8160 – 8169.
[36] S. Ashtekar, A. M. Prakash, L. Kevan, L. F. Gladden, *Chem. Commun.* **1998**, 91 – 92.
[37] S. Usseglio, P. Calza, A. Damin, C. Minero, S. Bordiga, C. Lamberti, E. Pelizzetti, A. Zecchina, *Chem. Mater.* **2006**, *18*, 3412 – 3424.
[38] L. Karwacki, E. Stavitski, M. H. F. Kox, J. Kornatowski, B. M. Weckhuysen, *Angew. Chem.* **2007**, *119*, 7366 – 7369; *Angew. Chem. Int. Ed.* **2007**, *46*, 7228 – 7231.

